

Seismic loss assessment of a structure retrofitted with slit-friction hybrid dampers



Jinkoo Kim*, Hyungjun Shin

Dept. of Civil and Architectural Engineering, Sungkyunkwan University, Suwon, Republic of Korea

ARTICLE INFO

Article history:

Received 3 March 2016

Revised 27 October 2016

Accepted 28 October 2016

Keywords:

Slit dampers
Friction dampers
Seismic retrofit
Life cycle cost
FEMA P-58

ABSTRACT

In this study a hybrid energy dissipation device is developed by combining a steel slit plate and friction pads to be used for seismic retrofit of structures, and its effectiveness is investigated by comparing the life cycle costs of the structure before and after the retrofit. A hybrid damper is manufactured and is tested under cyclic loading. It is observed that the damper shows stable hysteretic behavior throughout the loading history, and that the cumulative ductility ratio obtained from the experiment far exceeds the limit value required by the AISC Seismic Provisions. The probabilities of reaching various damage states are obtained by fragility analysis to evaluate the margin for safety against earthquakes, and the life cycle costs of the model structures are computed using the PACT (Performance Assessment Calculation Tool). According to the analysis results the slit-friction hybrid damper shows superior performance to the slit damper with the same yield strength for seismic retrofit of structures. The analysis results also show that the probabilities of reaching the limit states are minimized by the seismic retrofit with hybrid dampers combined with increasing column size. The combined seismic retrofit method also results in the lowest repair cost and shortest repair time.

© 2016 Elsevier Ltd. All rights reserved.

1. Introduction

Currently two of the most widely used seismic energy dissipation devices in building structures are metallic yield dampers and friction dampers. The metallic energy dissipative devices have been developed in many forms such as ADAS [1], buckling restrained braces [2], and slit dampers [3]. Among the metallic dampers, steel plate slit dampers have advantage in that they are relatively easy to design and manufacture [4–8]. Friction dampers have also been applied in various forms as presented in Pall and Pall [9] and Mualla and Belev [10]. Recently Lee et al. [11] developed friction dampers utilizing friction between low-steel composite material and milled steel.

Recently various energy dissipation devices or passive dampers have been widely applied for seismic retrofit of existing structures. Some researchers investigated simultaneous application of multiple devices to maximize the energy dissipation mechanism. For example, Tsai et al. [12], Chen et al. [13], and Uetani et al. [14] studied combined displacement-dependent and velocity-dependent devices for seismic mitigation of structures to minimize the shortcomings of individual dampers. Marko et al. [15] studied the effect of combined friction-viscoelastic damping devices strategically

located within shear walls and demonstrated the feasibility of mitigating the seismic response of building structures by using embedded dampers. Marshall and Charney [16] studied a hybrid system with buckling restrained braces and viscous fluid device by investigating the seismic response of steel frame structures. Optimum design procedures for hybrid or multiple dampers have been developed by Murakami et al. [17]. Lee and Kim [18] investigated the effectiveness of a hybrid damper consisting of steel slit plate and rotational friction devices to be used effectively both for small and large earthquakes. Lee et al. [19] investigated the combined behavior of shear-type friction damper and non-uniform strip damper for multi-level seismic protection. The results of the previous studies demonstrated the capability of hybrid passive systems to improve structural response compared with conventional lateral systems. The hybrid configuration improved some aspect of structural response providing benefits for multiple damage measures.

The purpose of this study is to develop a hybrid slit-friction damper which works for both major and minor earthquakes, and to investigate its validity by evaluating the life cycle cost of a structure before and after retrofit with the dampers. The hybrid damper is made of a steel slit damper and friction dampers connected in parallel. For minor earthquakes or strong winds, the slit damper remain elastic and only the friction damper yields to dissipate vibration energy, while for strong earthquakes both the friction

* Corresponding author.

E-mail address: jkim12@skku.edu (J. Kim).

and slit dampers work simultaneously to dissipate seismic input energy. Cyclic loading tests of the hybrid dampers are carried out to evaluate their seismic energy dissipation capability. The hybrid dampers are applied to seismic retrofit of an analysis model structure, and the effectiveness of the dampers is checked using fragility analyses to obtain the probability of four limit states being reached. Finally, loss estimation is carried out using the PACT (Performance Assessment Calculation Tool) program developed based on FEMA P-58 [20] methodology.

2. Development of a slit-friction hybrid damper

2.1. Property of the damper

The hybrid damper developed in this study consists of a steel slit damper to resist strong earthquakes and friction dampers to dissipate vibration energy caused by small earthquakes or strong winds connected in parallel as shown in Fig. 1(a). The friction pads are attached on both surfaces of the steel slit plate, and two side plates are placed at both sides of the slit plate. The two side plates are fastened together by high-tension bolts which go through the slotted holes in the slit plate so that the slit plate does not contact with the bolts. In practice the slit plate is connected to the structure at both the top and bottom so that it deforms to the inter-story drift, and the two side plates are only connected to the structure at the bottom so that friction force is generated by the relative movement between the slit plate and the side plates. A 1.0 mm-deep engraving is made on the surface of the slit plate where the friction pads are attached to prevent lateral movement of the friction pads and to restrain radial elongation of the pads due to the large clamping force applied by the high-tension bolts. To evenly distribute the clamping force on the surface of the friction pads, the rectangular plates are inserted between the bolt head or the nut and the steel side plates. The overall width and height of the steel plate are 500 mm and 700 mm, respectively. The plate has nine slit columns: the width (b), thickness (t), and the height (l_0) of each slit column are 20 mm, 15 mm, and 200 mm respectively, as depicted in Fig. 1(b). The stiffness and yield strength of a slit damper can be derived based on elementary mechanics of materials as follows [3]:

$$k_s = n \frac{12EI}{l_0^3} = n \frac{Etb^3}{l_0^3} \quad (1a)$$

$$P_y = \frac{2nM_p}{l_0} = \frac{n\sigma_y tb^2}{2l_0} \quad (1b)$$

where n = number of strips, M_p is the plastic moment of a strip, σ_y is the yield stress of the plate, t = thickness of strips, b = width of strips, and l_0 = length of the vertical strip.

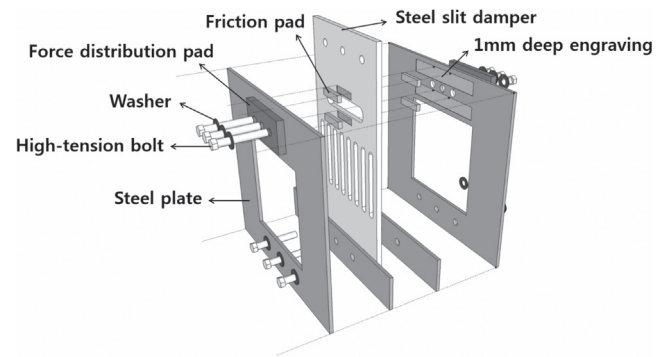
The yield force of the friction dampers is proportional to the clamping force N and the friction coefficient μ as follows:

$$P_{yf} = \mu \times N \quad (2)$$

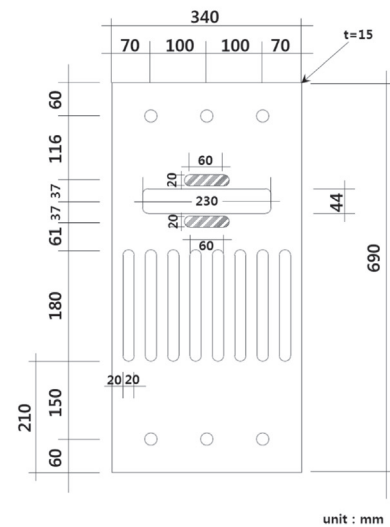
In the case the slit damper and the friction damper are connected in parallel, the yield strength of the hybrid damper can be calculated as follows:

$$P_y = \left(\frac{n\sigma_y tb^2}{2l_0} \right) + \mu N \quad (3)$$

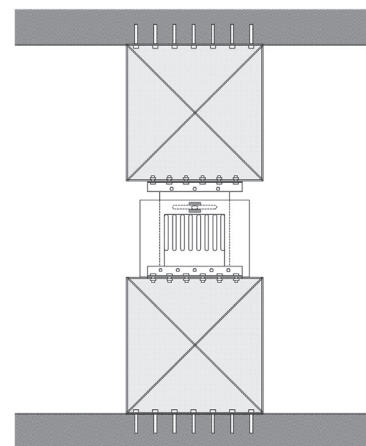
The hybrid damper is basically a displacement-dependent device which dissipates seismic energy by yielding of steel slits (slit dampers) and slip of friction pads (friction dampers). The slip of friction pads occurs at small lateral displacement, which makes



(a) Components of hybrid damper



(b) Dimension of slit plate



(c) Typical installation scheme

Fig. 1. Configuration of the proposed slit-friction hybrid damper.

it effective in resisting small earthquakes and strong wind loads. The slit dampers remain elastic during small earthquakes and are activated at major earthquakes.

Such dampers are generally located inside of partition walls. The damper unit is placed between two strong frames as shown in Fig. 1(c); the upper strong frame is fixed to the upper beam and the lower one is fixed to the lower beam. The strong frame can be made of rectangular steel plate with diagonal stiffener or rectangular frame with diagonal or X-shaped steel bracing, which

is strong enough to behave like a rigid body during earthquakes. When inter-story drift occurs during earthquakes, only the damper unit yields and dissipates hysteretic energy while the strong frames remain almost undeformed. For retrofit of existing RC structures, chemical anchors are installed in the upper and the lower beams and the strong frames are fixed to the structure using the anchor bolts. To install the dampers in new RC structures anchor bolts are embedded in beams before pouring of concrete and the remaining steps are the same. In steel buildings the strong frames can be bolted or welded to the beams.

2.2. Cyclic loading tests of the damper

Displacement-controlled cyclic tests of the specimens are carried out using a 500 kN hydraulic servo actuator to evaluate the seismic performance of the hybrid damper. Fig. 2 depicts the test setup for the cyclic loading test, and Fig. 3 shows the photographs of the friction damper and the hybrid damper installed inside of the strong frame. LVDT (linear variable differential transformer) is installed to measure the horizontal displacement of the specimens during experiments. In the test of the friction damper, two exterior plates are fixed at the bottom strong floor and are free at the top. The interior plate with friction pads at both faces, which is separated from the bottom floor, is moved by the actuator so that only the friction force is activated due to the relative movement of the interior and the exterior plates. For the test of the friction damper 10 cycles of harmonic loading is applied as shown in Fig. 4(a) in such a way that the maximum displacement of 65 mm is reached at each loading cycle which corresponds to 2.2% of the story height. The loading protocol is specified in the FEMA-461 [21] for quasi-static cyclic loading tests. The friction coefficient μ of the friction pads used in the hybrid damper is determined to be 0.5 based on a series of preliminary tests measuring slip force of the friction pad subjected to various clamping forces induced by a torque wrench. The high-tension bolts used to provide clamping force on the friction pads have the tensile strength of 165 kN with diameter of 20 mm. Each friction damper is fastened by the high-tension bolts with three different pretensions (50 kN, 75 kN, and 100 kN) imposed on the friction pads. The hybrid damper is composed of the slit damper shown in Fig. 1(b) and the friction damper with clamping force of 75 kN. From Eqs. (1) and (2) the yield force of the slit damper and the slip force of the friction damper are estimated to be 48.8 kN and 37.5 kN, respectively. This combination of two dampers results in yield strength of the hybrid damper of 86.3 kN as obtained from Eq. (3). When the shear force imposed on the hybrid damper exceeds the slip force of 37.5 kN, the slip

damper is activated and dissipate hysteretic energy while the slit damper will remain elastic until the shear force reaches the combined yield strength of 86.3 kN. When the applied shear force reaches the combined yield strength of the hybrid damper, both the friction and the slit damper work together to dissipate seismic energy. In practice the proper slip force of the friction damper can be determined from preliminary analysis of the structure subjected to minor earthquakes (earthquakes with return period of 200 years, for example). For the test of the hybrid damper the bottom of the slit plate is fixed at the strong floor and the top of the plate is moved by the actuator. The minimum displacement (Δ_0) of the loading protocol is determined to be 4.5 mm which corresponds to 0.15% of the inter-story drift in a structure with 3 m story height. After each two cycles of loading, the displacement amplitude is increased to 1.4 times the previous one until the maximum displacement of 65 mm is reached.

To verify the energy dissipation capacity of the friction damper, cyclic loading tests are carried out with the lower half part of the central slit plate shown in Fig. 1(b) removed. Fig. 5 shows the test results of the friction dampers with three different clamping forces using the loading protocol presented above. The slip force of each test is 25.1 kN, 37.8 kN, and 50.4 kN, respectively, for the imposed clamping force of 50 kN, 75 kN, and 100 kN. It can be observed that the slip force of the friction damper varies almost linearly with the friction coefficient of 0.5 following Eq. (2). It also can be noticed that the friction damper generates almost identical rectangular hysteresis loops for each loading cycle. The hysteresis curve of the hybrid damper is presented in Fig. 6(a). The yield strength of the hybrid damper turns out to be 84.5 kN which is slightly lower but quite similar to the yield force predicted by Eq. (3). It is observed during the test that fracture of a slit column occurred first at the 17th loading cycle and strength dropped after the 18th cycle. Jigs used in this test allow little vertical displacement at large lateral drift and induce diagonal tension field, which results in further increase of post-yield strength at lateral displacement higher than 30 mm as can be observed in the hysteresis curves. The increase in strength due to formation of tension field in steel hysteretic dampers can also be observed in Whittaker et al. [22]. The envelop curve is idealized by a series of linear lines for nonlinear analysis as depicted in Fig. 6(b). AISC Seismic Provisions [23] requires that the cumulative ductility ratio of a hysteretic device be larger than 200. In this study the cumulative ductility ratio of the hybrid damper turns out to be 295, which confirms that the damper has enough plastic deformation capability. Table 2 shows the properties of the hybrid damper obtained from the experiment and from Eqs. (1)–(3).

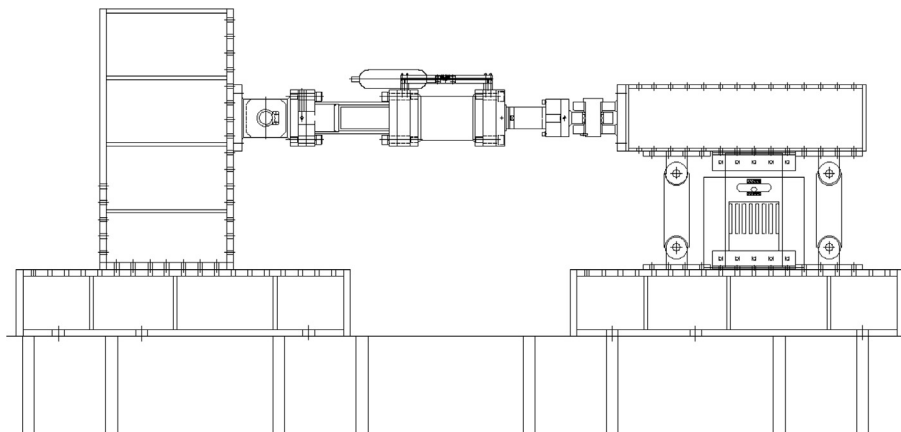


Fig. 2. Test setup for loading test of the slit-friction hybrid damper.

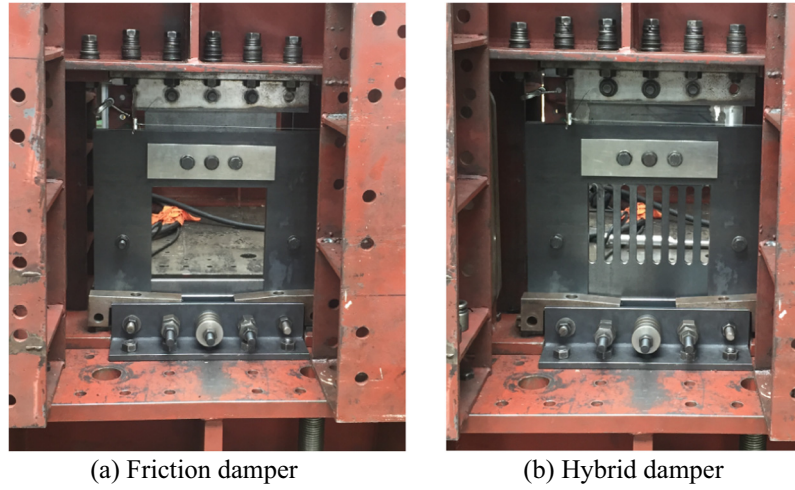


Fig. 3. Specimens installed for test.

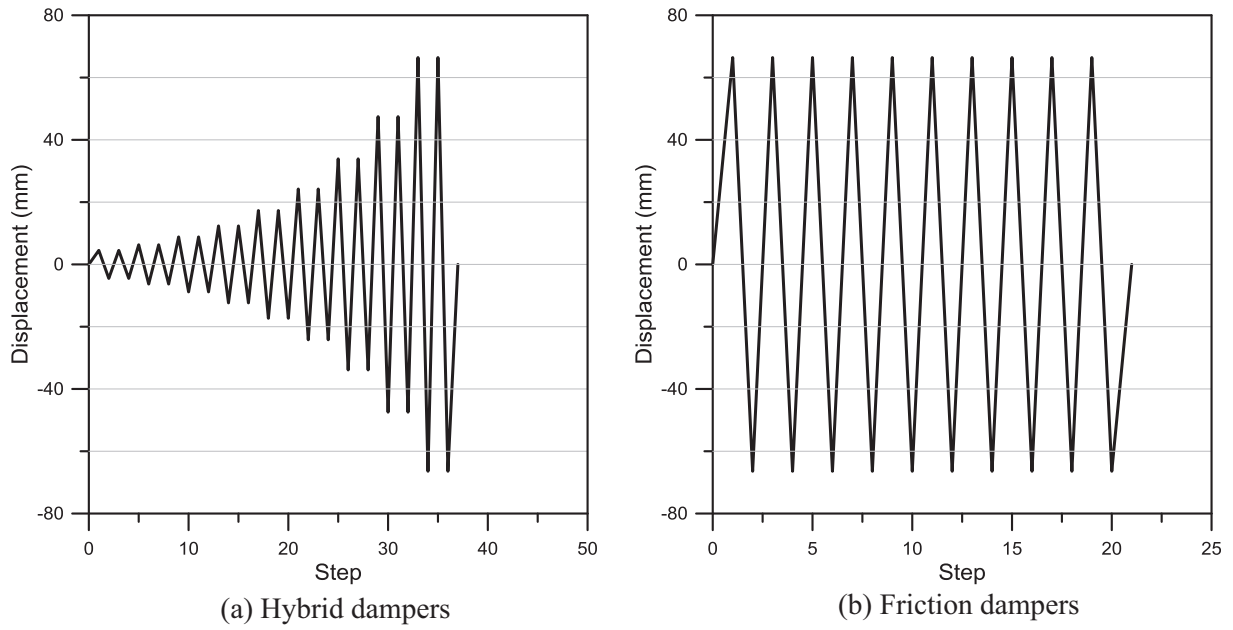


Fig. 4. Loading protocols used in the experiments.

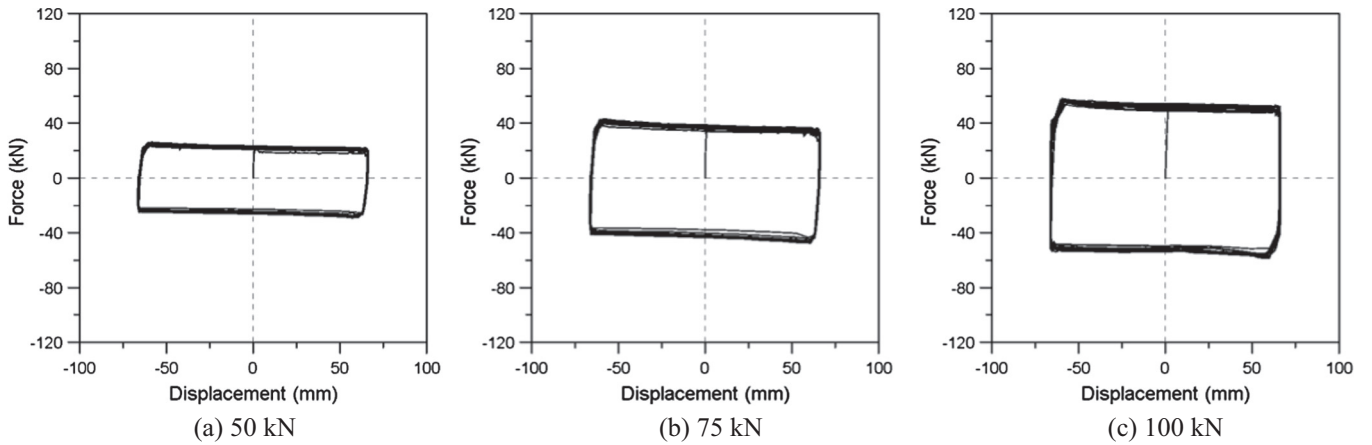


Fig. 5. Force-displacement curves of friction dampers with different bolt tensions.

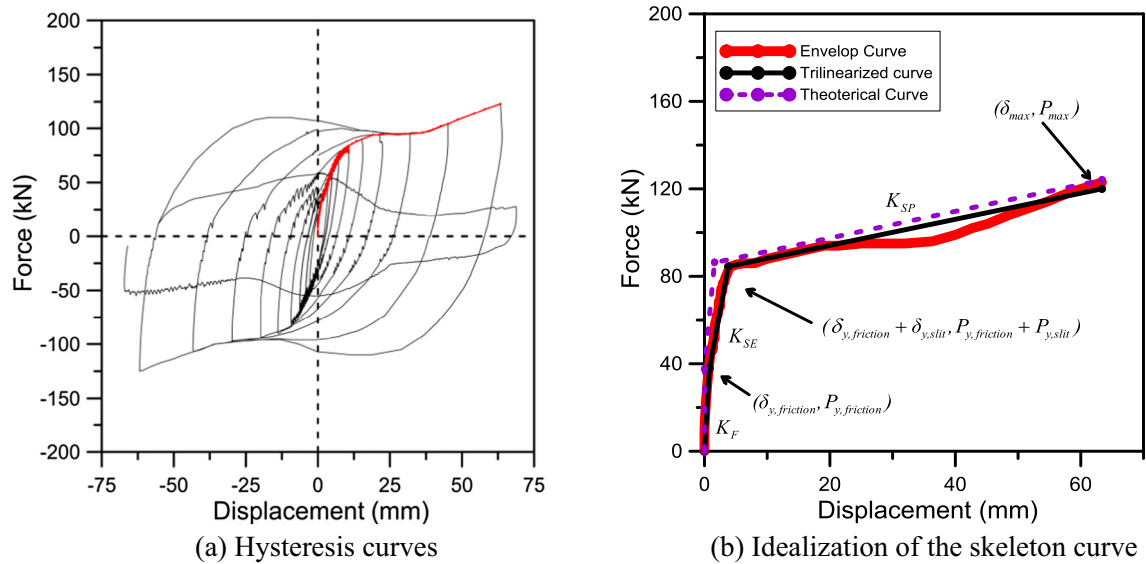


Fig. 6. Test results of the hybrid damper.

Table 1
Section size and rebar placement of the model structure.

Name	Column size (mm × mm)	Main bars	
<i>(a) Column size and main rebars</i>			
1-CA1	350 × 400	8D19	
1-CA2-3	350 × 600	8D29	
1-CA4	350 × 550	8D25	
1-CA5-6	350 × 600	8D29	
1-CA7	350 × 500	8D25	
1-CB1	350 × 600	8D25	
1-CB2-3	350 × 1000	12-3 D29	
1-CB4	350 × 1000	12-3 D29	
1-CB5-6	350 × 1200	12-3 D32	
1-CB7	350 × 900	12-3 D29	
Name	Beam size (H × B) (mm × mm)	Arrangement of rebars	
		Exterior (I,J)	Interior (M)
<i>(b) Beam size and rebar arrangement</i>			
1-GA	250 × 250	2-D16	2-D16
1-GB	330 × 300	2-D19	2-D19
1-GC	250 × 250	2-D16	2-D16
1-B1	330 × 350	4-D22	2-D22
1-B2-6	350 × 350	6-D22	4-D22
1-B7	330 × 350	6-D22	2-D22

Table 2
Properties of the hybrid damper obtained from experiments and analytical models.

	Theoretical values	Experimental results
$(\delta_{y,friction}, P_{y,friction})$	(0 mm, 37.5 kN)	(0.8 mm, 37.8 kN)
$(\delta_{y,slit}, P_{y,slit})$	(1.6 mm, 48.75 kN)	(3.0 mm, 46.7 kN)
(δ_{max}, P_{max})	(65.0 mm, 124.8 kN)	(63.38 mm, 120.0 kN)
K_{SE} , Elastic stiffness of slit dampers	30.66 kN/mm	15.57 kN/mm
K_{SP} , Post-yield stiffness of slit dampers	0.61 kN/mm	0.60 kN/mm

3. Seismic retrofit of an example structure

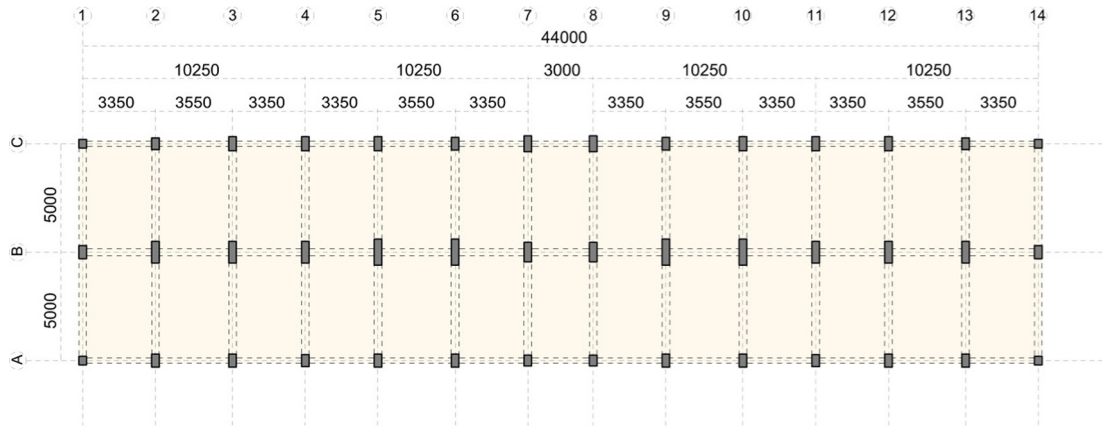
3.1. Description of the model structure

In this section the hybrid damper developed in this study is applied to seismic retrofit of an existing structure which is not designed considering seismic load. The analysis model structure

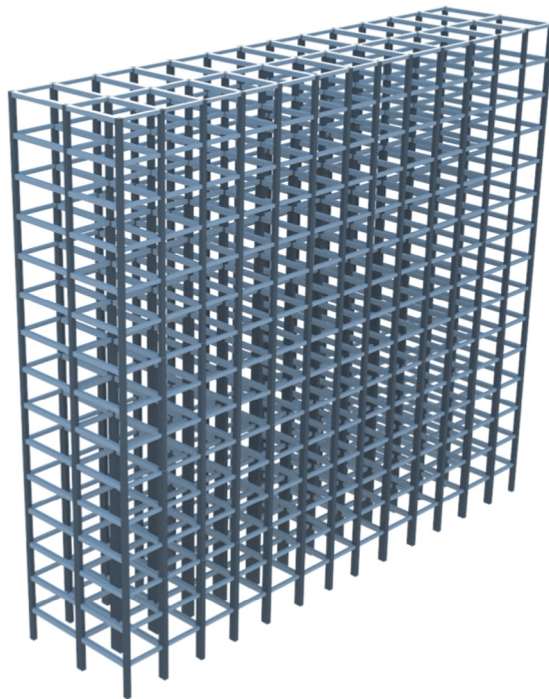
is a 15-story reinforced concrete apartment building built in early 1970s. The structure is composed of moment resisting frames in both directions and has uniform story height of 2.65 m. The structure has a rectangular plan shape with 5 m span length along the transverse direction and 3.35 m and 3.55 m span length along the longitudinal direction as shown in Fig. 7(a). As the wind load is the main lateral load, the longer dimension of the columns is located along the transverse direction in which the wind load is larger. The exterior corridor and the balcony, which are cantilevered from the slab along the longitudinal direction, are not considered in the structural modeling, but are included as line load along the perimeter. The slabs are assumed to be rigid diaphragm and the strengths of reinforced concrete and re-bars are assumed to be 21 MPa and 240 MPa, respectively. The size and re-bar placement in the structural elements in the first story are shown in Table 1. The fundamental natural period of the model structure turns out to be 3.7 s along the longitudinal direction and 3.1 s along the transverse direction.

3.2. Modeling for nonlinear analysis

The seismic performance of the model structure is evaluated using the seismic performance criteria of ASCE/SEI 41-13 [24]. The nonlinear bending moment vs. rotation relationships of columns are represented by tri-linear lines as shown in Fig. 8. The post yield stiffness varies depending on the axial force as specified in the ASCE/SEI 41-13. Following the recommendation of ASCE/SEI 41-13, the over-strength factors of 1.5 and 1.25 are applied for the strength of reinforced concrete and re-bars, respectively. The effective stiffness of the beams and columns in elastic range is reduced to $0.5E_cI_g$ and $0.7E_cI_g$, respectively, considering cracked section. The shear strength of the elements is reduced to $0.4E_cA_w$. Nonlinear static and dynamic analyses are carried out using the program code Perform 3-D [25]. The behavior of the hybrid damper is modeled using the 'Rubber Type Seismic Isolator Element' which resists both axial and shear forces and can be used to model hysteretic damping devices as well as seismic isolators. The element has been successfully applied to model the behavior of slit dampers used for seismic retrofit of existing structures [18,26].



(a) Plan view



(b) 3-D view

Fig. 7. Shape of the example structure.

3.3. Evaluation of the required damping

It is observed in the preliminary analysis that there is enough strength to resist the design seismic load along the transverse direction; however little lateral load resistance exists along the longitudinal direction. For seismic retrofit of the model structure a target performance point is evaluated first, and then the required damping ratio to satisfy the target performance point is computed using the capacity–demand diagram method provided in the ATC-40 [27] Procedure B. Finally the slit or hybrid dampers are installed to provide the required damping and to limit the seismic performance within the desired target performance point.

To obtain capacity curve, pushover analysis is carried out along the longitudinal direction using the lateral load proportional to the fundamental mode shape of the structure. The lateral load is gradually increased until the roof displacement reaches 4% of the building height, and the base shear vs. roof displacement curve is obtained. The design spectrum corresponding to the 2/3 intensity

of the earthquake with 2400 year return period is constructed based on the ASCE 7-13 [28] format using the spectral acceleration coefficients for short period (S_{DS}) and 1 s period (S_{D1}) equal to 0.37 and 0.15, respectively. Then the pushover curve and the design spectrum are converted to the ADRS (acceleration displacement response spectrum) format using the procedure recommended in the ATC 40 Procedure B as shown in Fig. 9. The target displacement δ_t is computed using the following formula presented in the FEMA 41-13 [24]:

$$\delta_t = C_0 C_1 C_2 C_3 S_a \frac{T_e^2}{4\pi^2} g \tag{4}$$

where the modification factor C_0 , C_1 , C_2 , and C_3 are determined to be 1.5, 1, 1, and 1, respectively. T_e is the effective fundamental period of the structure computed to be 3.6 s, and S_0 is the response spectrum value at the effective fundamental period obtained as 0.04 g where g is the acceleration of gravity. Using the above

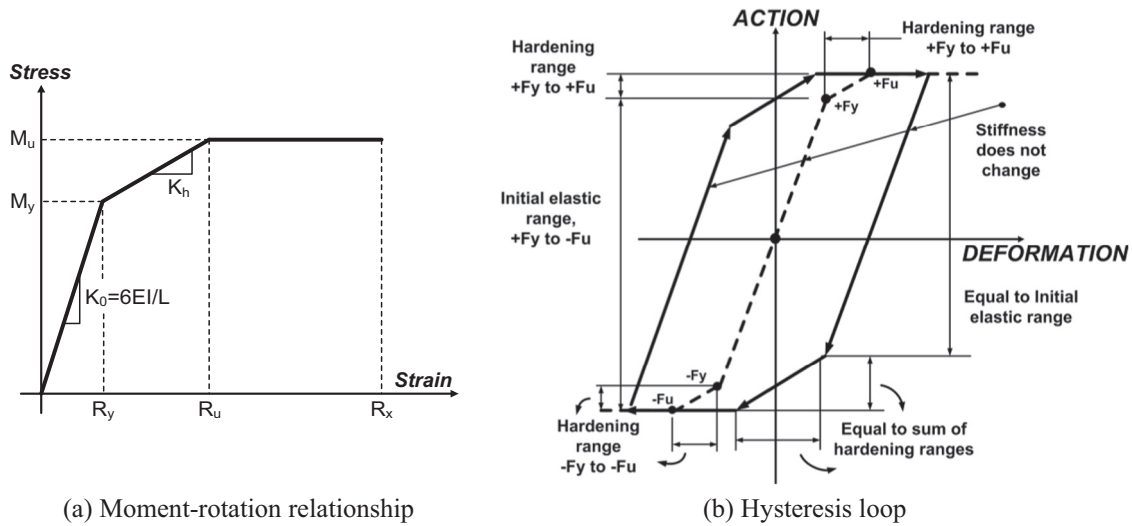


Fig. 8. Nonlinear model for columns.

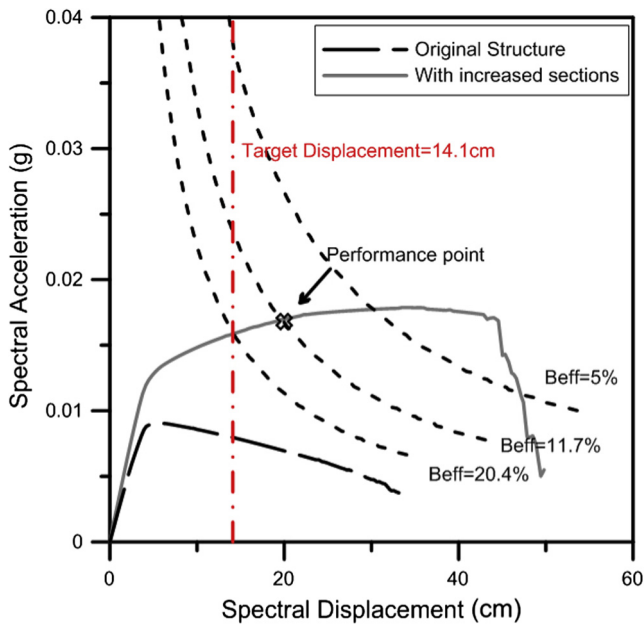


Fig. 9. Computation of the required damping to achieve the target response using the capacity spectrum method.

equation δ_i is computed to be 19.5 cm, which is converted to the spectral displacement of 14.1 cm. The maximum inter-story drift corresponding to the spectral displacement is 0.8% of the story height. It can be noticed in the figure that the demand curve is still above the capacity curve of the original structure even at the effective damping of 20% which is considered as the practically meaningful upper limit. In this case it would be more economical to increase the inherent strength of the structure until the capacity curve meets with the demand curve at the target point, and to provide the effective damping of 20% by installing dampers. To increase the inherent strength of the structure, the short sides of the columns are increased by up to 20 cm so that the capacity curve meets with the demand curve corresponding to the effective damping of 20% at the target performance point as shown in the figure. The sizes of the 1st story columns in the retrofitted structure are shown in Table 3.

With the required effective damping of 20% obtained in the capacity spectrum method to satisfy the target performance point, the dampers are designed using the formula presented in the ASCE/SEI 41-13:

$$\beta_{eff} = \beta + \frac{\sum W_j}{4\pi W_k} \quad W_k = \frac{1}{2} \sum F_i \delta_i \quad (5)$$

where β is the inherent damping assumed to be 5% of the critical damping, W_j is the hysteretic energy dissipated by the dampers in the i th story, W_k is the potential energy of the structure, F_i is the design seismic story shear at the i th story, and δ_i is the target inter-story drift of the i th story.

To increase the effective damping of the structure, the hybrid dampers developed in this study are applied. Slit dampers having the same strength with the hybrid dampers are also used for comparison. As the properties of the hybrid damper, which varies depending on such factors as geometry, yield stress, clamping force, etc., are easily obtained from formulas, the yield force of the dampers used in the analysis is arbitrarily determined to be 48.8 kN. Using Eq. (5) the number of slit or hybrid dampers to satisfy the required effective damping is estimated to be 21. Two dampers are installed at each story from the 2nd to the 10th story and one per story from the 11th to the 13th story, as shown in Fig. 10(a). For comparison, the number of dampers required to meet the target displacement without increase of member size is estimated to be 66, the location of which are shown in Fig. 10(b). As the beam size of this residential building used as analysis model structure is quite small compared with that of typical RC office

Table 3
Size of columns in the retrofitted structure.

Name	Size (mm)	Main bars
1-CA1	550 × 400	8D19
1-CA2-3	550 × 600	12D19
1-CA4	550 × 550	6D25
1-CA5-6	550 × 600	12D19
1-CA7	550 × 500	10D19
1-CB1	550 × 600	12D19
1-CB2-3	550 × 1000	20D19
1-CB4	550 × 1000	20D19
1-CB5-6	550 × 1200	16D25
1-CB7	550 × 900	10D25

buildings, large number of dampers with relatively small unit yield strength are used for seismic retrofit instead of small number of dampers with high yield strength.

Fig. 11 shows the pushover curves of the model structure before and after the retrofit, where it can be observed that the strength of the model structure is significantly increased after the retrofit. The structures retrofitted with the 21 slit dampers (SD) and hybrid dampers (HD) accompanied with increase of column size (IS) show much larger ductility than the structures retrofitted with 66 dampers without increase of column size. It is observed that in the structure retrofitted only with the dampers, plastic rotations exceeding the CP (collapse prevention) state occur at most of the lower story columns which leads to rapid drop of the overall strength. The strength and ductility of the structures retrofitted with the slit and the hybrid dampers having the same ultimate strengths are similar to each other.

For nonlinear dynamic analysis of the model structures, seven artificial earthquake records are generated to match the design spectrum. The response spectra of the records and the design spectrum are shown in Fig. 12. Fig. 13(a) and (b) depict the mean maximum story displacements and inter-story drifts of the model structures, respectively, obtained from time history analysis using the seven artificial earthquake records. The story displacement results of the model structure show that the overall displacement of the model structure including the roof-story displacement is significantly reduced after the seismic retrofit. It can be noticed that the story displacement shapes of the retrofitted structures become closer to linear lines compared with the displacement shape of the structure without retrofit. It also can be observed that the maximum inter-story drifts of the original structure far exceed 1.0% of the story height which is considered as the Life Safety performance limit state for residential apartment buildings when they are subjected to the design level seismic load. However the inter-story drifts of the retrofitted structures turn out to be less than the limit state.

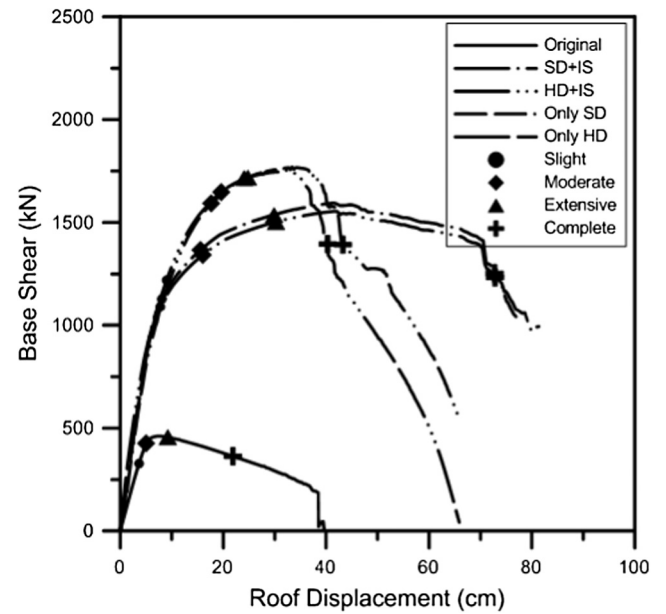


Fig. 11. Pushover curves of the model structures with indication of four damage states.

4. Fragility analysis of model structures

Seismic fragility is the conditional probability that the structural capacity, C , fails to resist the structural demand, D , given the seismic intensity hazard, and is modeled by a lognormal cumulative distribution function as follows [29]:

$$P[D \geq C] = \Phi(\ln[D/\hat{C}]/\beta_c) \tag{6}$$

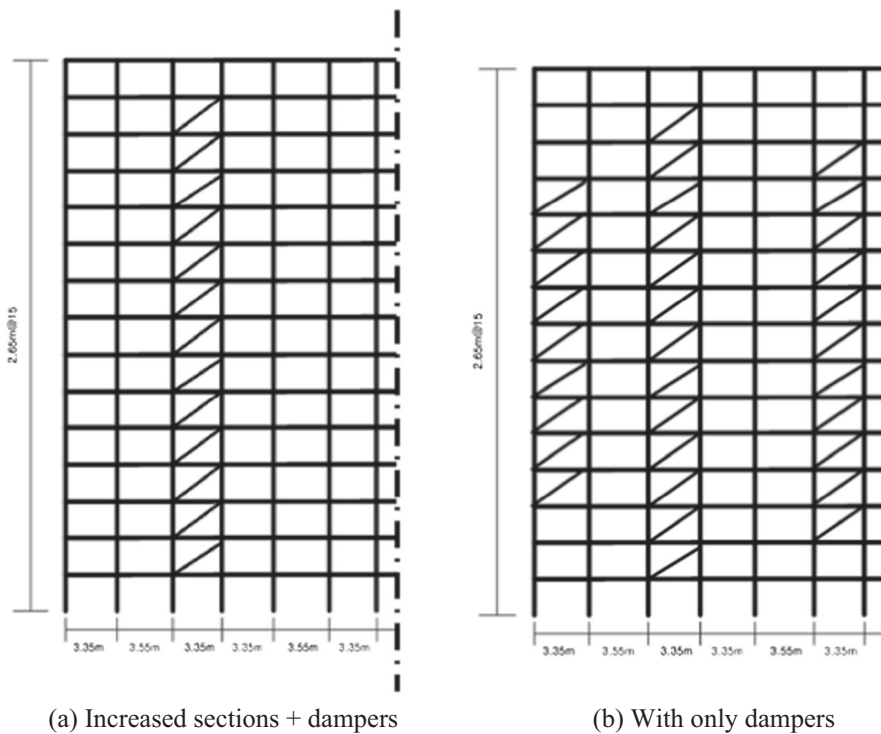


Fig. 10. Location of dampers installed for seismic retrofit.

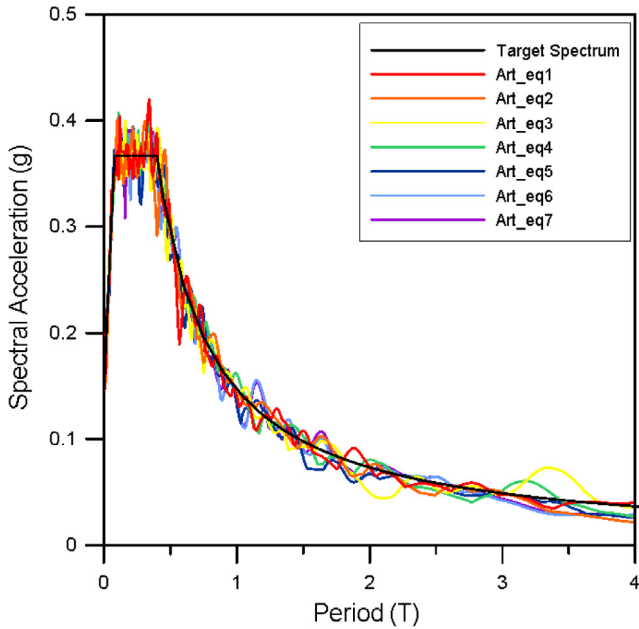


Fig. 12. Response spectra of the seven artificial earthquake records.

where $\Phi[\cdot]$ = standard normal probability integral, \hat{C} = median structural capacity, associated with the limit state, and β_C = uncertainty in C .

To obtain seismic fragility of the model structure, incremental dynamic analyses are carried out using the twenty-two pairs of scaled far-field records provided by the PEER NGA Database [30]. Fig. 14 depicts the incremental dynamic analysis results of the model structures using the 44 earthquake records. The spectral acceleration at which dynamic instability of the structure occurs for more than 22 earthquake records is also indicated in the figures. In this study the state of dynamic instability is defined as the point at which the stiffness decreases lower than 20% of the initial stiffness in the incremental dynamic analysis. It can be observed that the median spectral acceleration at dynamic instability increases from 0.2 g in the original structure to 0.6 g in the

structure with increased column section plus hybrid dampers. Even though the slit and the hybrid dampers have the same strength, the median failure spectral accelerations of the structures with hybrid dampers are slightly higher than those of the structures with the slit dampers.

Based on the incremental dynamic analysis results, probabilities of reaching the four damage states defined in the HAZUS [31], which are Slight, Moderate, Extensive, and Complete damage, are computed. The Complete damage state is defined as the maximum inter-story displacement at which the strength decreases to 80% of the maximum strength in the pushover curve. The states of the Slight damage and the Moderate damage were defined as the spectral displacements corresponding to the 70% and the 100% of the yield point, respectively. The Extensive Damage was defined as the quarter point from the Moderate to the Complete damage. Fig. 15 depicts the fragility curves of the analysis model structures, where it can be observed that the structures designed with friction dampers have significantly lower probability of reaching the collapse state than the strength-designed structure. The spectral acceleration corresponding to the 50% probability (the median structural capacity) of reaching the Slight damage state turns out to be highest value of 0.08 in the structure retrofitted only with hybrid dampers, followed by the structure with only slit dampers. This implies that for a given spectral acceleration the probability of reaching the limit state is lowest in the structure retrofitted with hybrid dampers. The probabilities of reaching the Moderate damage state show similar trend, except that the difference between the probabilities in the original and the retrofitted structures becomes larger. For Extensive damage state the failure probability is the lowest in the structure with only hybrid dampers followed by the structure retrofitted with hybrid dampers after increase in column size. The probability of reaching the Complete damage state is the lowest in the structure retrofitted with hybrid dampers combined with increase of column size, followed by the retrofit only with hybrid dampers. Next come the retrofit with slit dampers plus increase of column size and the retrofit with only slit dampers. In summary, it is observed that the installation of the hybrid dampers turns out to be the most effective in the Slight, Moderate, and the Extensive damage states, whereas in the Complete damage state the retrofit with hybrid dampers combined with increase of column size results in the best solution.

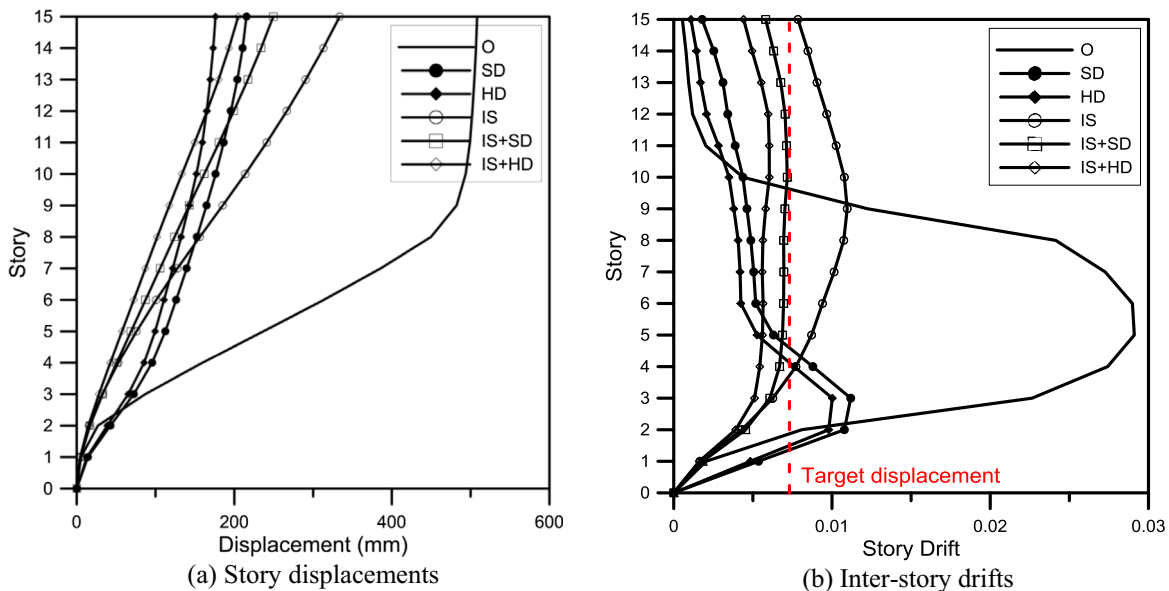


Fig. 13. Displacement response of the model structures retrofitted with various methods averaged over seven time history analysis results.

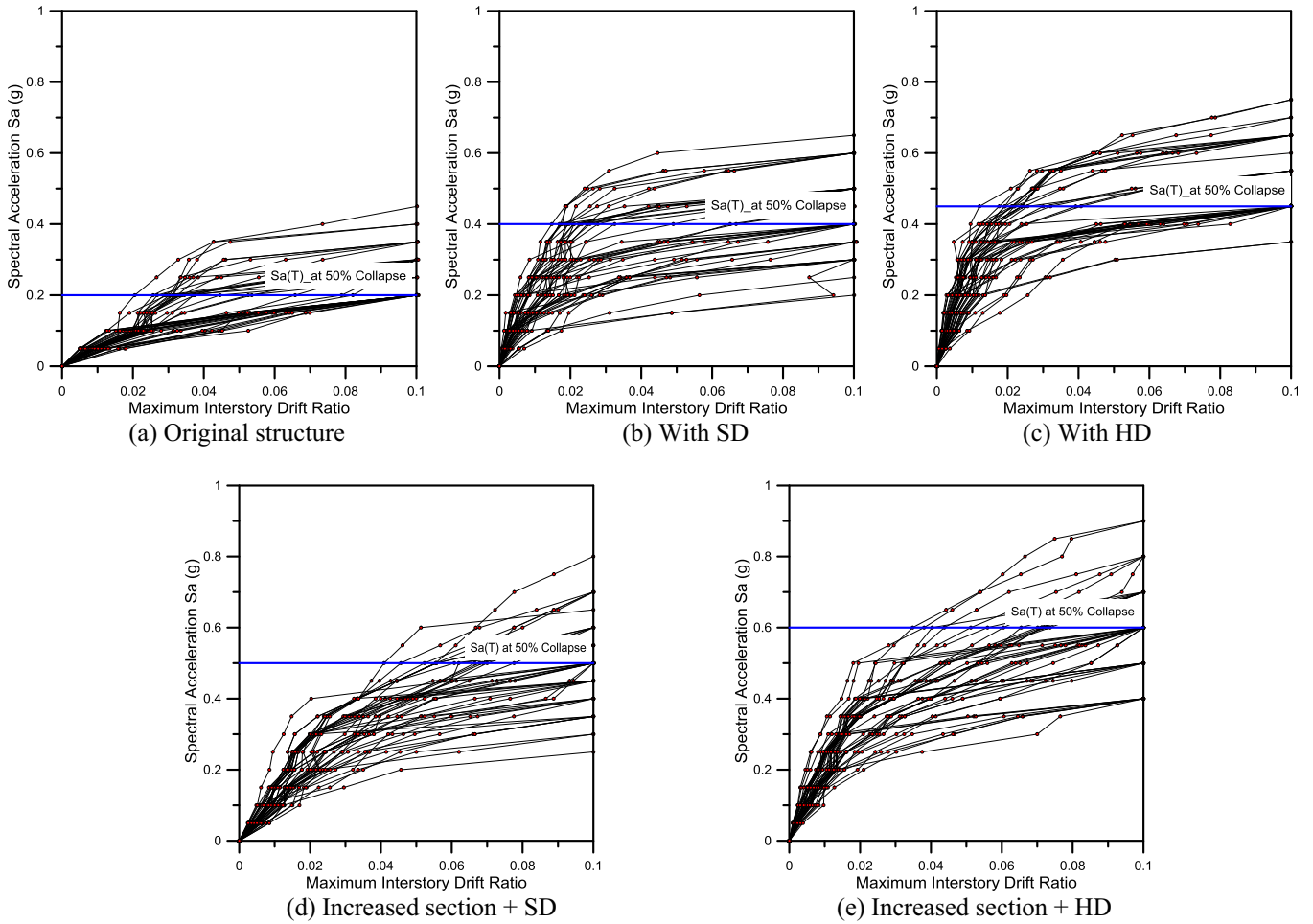


Fig. 14. Incremental dynamic analysis results of the model structures.

5. Life cycle cost evaluation of the model structures

5.1. FEMA P-58 method

FEMA P-58 [20] is a process that quantifies the performance measures of a structure in terms of casualties, repair cost, repair time, etc. The methodology includes a computer program (Performance Assessment Calculation Tool, PACT) which can be used to carry out seismic performance assessment of buildings to estimate performance measures such as losses. The FEMA P-58 assessment process starts from assembling the building performance model and defining the earthquake hazards for the site. Then the building response to earthquake ground excitation and a collapse fragility curve are assessed to predict the probable damage for different shaking intensities.

In the FEMA P-58 method the repair costs and time are determined as distributions of the likely consequences of damage translated into potential repair and replacement costs, repair time, casualties, etc. In this study the damage of dampers is divided into three states, DS1 to DS3. The repair cost and time of a slit damper in the DS1 damage state are determined as those required for unit price and placement of a damper, respectively. In the DS2 damage state the repair costs and time are evaluated as those for complete replacement of the damping system including the damper and the steel bracing with anchor bolts needed to attach the damper to the structural members. For the hybrid dampers the repair costs and time for DS1 are considered to be those for replacing friction pads. The repair costs and time for DS2 and DS3 are those needed to

replace the hybrid dampers and the bracing with anchor bolts, respectively. The repair costs and time for each damage state are shown in Table 4. In the FEMA P-58 method, the uncertainties involved in the prediction of seismic performance are accounted for by means of Monte Carlo simulation. FEMA P-58 recommends minimum number of 500 realizations. Structural modeling uncertainties are accounted for by defining a value of dispersion to the building definition and the analytical model. In this study the total structural modeling dispersion is assumed as 0.354 based on the construction quality assurance, β_c , of 0.25 and the quality of the analytical model, β_q , of 0.25. The two parameters are combined by SRSS method, which is used as input to the PACT analysis.

5.2. Loss and downtime assessment

In this study the life cycle cost and repair time of the structure with slit and hybrid dampers are compared at three levels of earthquake intensity, which have annual probability of exceedance of 50%, 5%, and 2% in 50 years. They correspond to earthquakes with mean annual exceedance frequency of 0.01, 0.001, and 0.0004, respectively. The design spectra of the seismic loads corresponding to the three intensity levels are shown in Fig. 16 constructed in the format of ASCE 7-13. The estimations for replacement cost shown in Table 5 are based on data from International Construction Cost Survey 2010–2011 [32] which contains construction cost per square meter for residential apartments in Korea. In the case of total collapse, the replacement cost of the original structure is

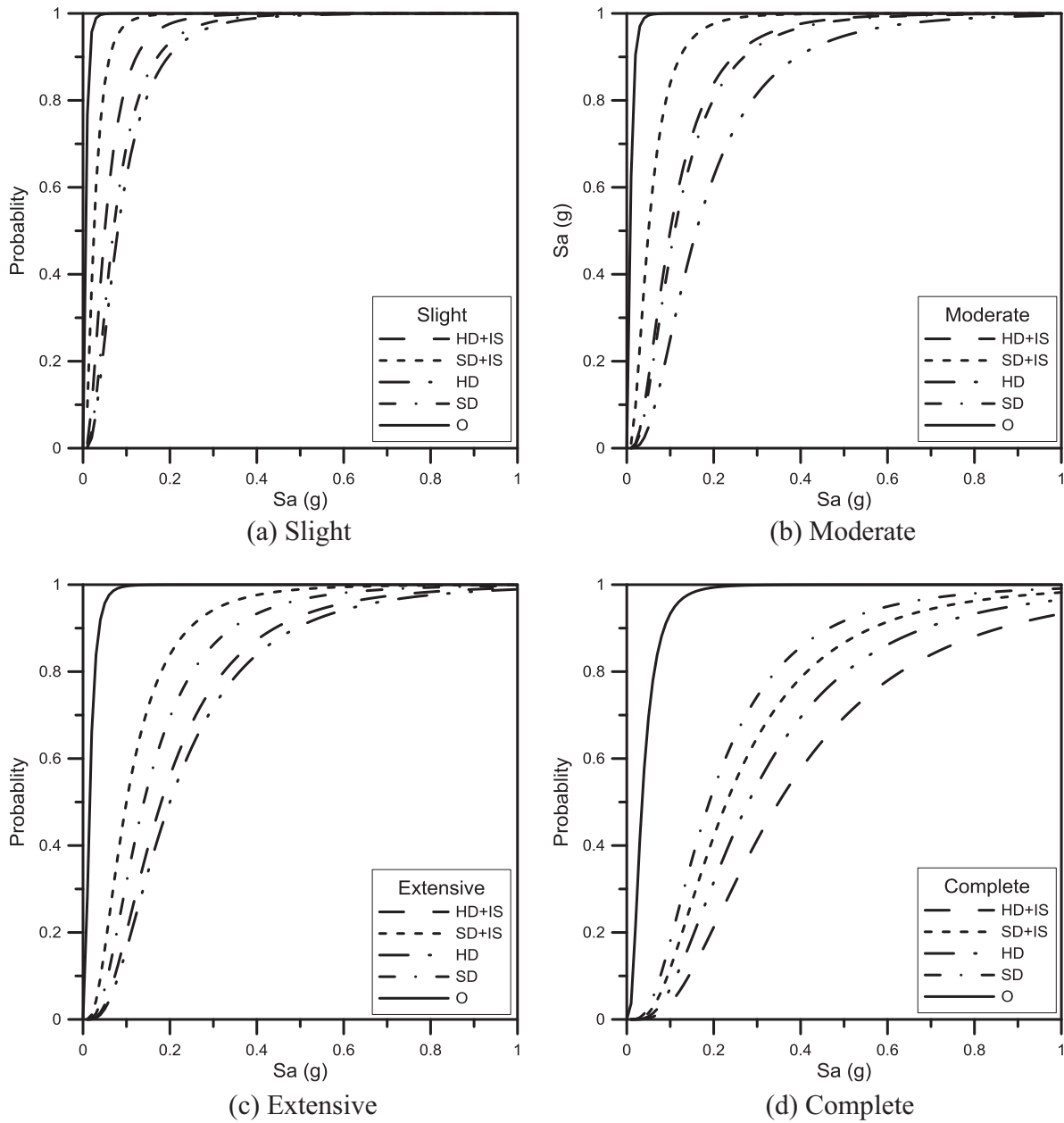


Fig. 15. Fragility curves for four damage states.

Table 4
Repair costs and repair time of slit dampers and hybrid dampers at each damage state.

	DS1		DS2		DS3	
Slit dampers	\$1000	3 days	\$2000	7 day		
Hybrid dampers	\$500	3 days	\$1500	3 days	\$2500	7 days

taken as \$ 6,712,200 which is calculated using the cost per unit area of \$1017/m². The required cost for increasing column size is estimated based on the RSMears Building Construction Cost Data 2011 [33]. The unit costs for the slit and the hybrid dampers are estimated to be \$2000 and \$2500, respectively, including labor cost for installation. Tables 6 and 7 show the total replacement cost and time for each model structure at each damage state. As these costs are specific to a country, only the relative value is important in the comparison of the repair costs of the building retrofitted with various methods. The total loss threshold is assumed to be the PACT

default value of 1.0. The construction period is assumed to be 200 days for the original structure and 215 days for the structure retrofitted with dampers. The use of the model structure is the residential apartments, and the population model uses the data corresponding to the 'Multi-unit Residential' in the PACT. The non-structural component fragilities are chosen based on this occupancy type with the aid of the Normative Quantity Spreadsheet provided in the FEMA P-58. In the fragility data the damage state is defined as the inter-story drift ratio. The damage state DS1 in the slit dampers is set to be the ratio of the yield displacement of

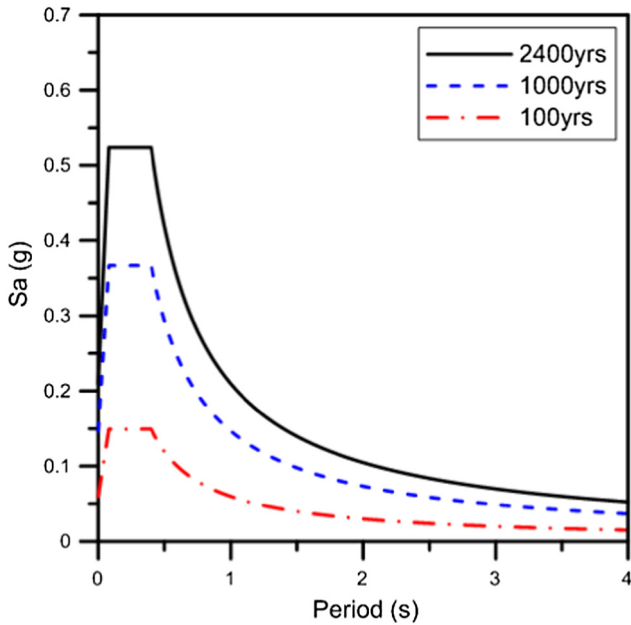


Fig. 16. Design spectra for earthquakes with three different return periods.

1.5 mm and the story height of 2650 mm. The damage state DS2 is defined as the ratio of the fracture displacement of the slit dampers, 65 mm, with the story height. The DS1 of the hybrid dampers is the ratio of the slip displacement of the friction pad, 0.5 mm, and the story height. The damage states DS2 and DS3 are considered as the yield and fracture displacements of the slit dampers divided by the story height. The variance is determined to be 0.187 based on the information provided in the section 3.8.4 of the FEMA

P-58 such as ductile failure modes, ASTM A36 steel, and moderate sensitivity. The variance of the damage state DS2 or DS3 is set to be the same with that of DS1.

To obtain the statistical data on the inter-story drifts and the story accelerations, nonlinear dynamic analyses are carried out using the 11 earthquake records provided by the PEER NGA Database [27]. The records are scaled in such a way that the spectral accelerations of the records corresponding to the fundamental natural periods of the model structures along the longitudinal direction become equal to those of the design spectra for earthquakes with return period of 100, 1000, and 2400 years. The analysis results are input to the PACT software which carries out Monte Carlo simulation to generate 500 realizations for inter-story drifts and story accelerations. Fig. 17(a) shows the maximum inter-story drifts of the first story (δ_1) and the second story (δ_2) obtained from the dynamic analysis using the earthquake records with Intensity I (original data) and from the Monte Carlo simulation (simulated data). Similar results are plotted in Fig. 17(b) for the acceleration of the first story (a_1) and the second story (a_2). Fig. 18 shows the mean story drifts of the 500 simulated realizations obtained for the seismic intensities 1 and 3. Story drifts are an important consideration when estimating losses. For each realization, the PACT analysis uses the maximum story drift together with the building repair fragility to determine the damage state. If the structure turns out to be irreparable, repair cost and repair time are taken as the building replacement values.

The cumulative distribution of 500 realizations of repair costs and time computed using the PACT software are depicted in Figs. 19 and 20, respectively, for the original and the retrofitted structures. Fig. 19 shows the relationship between the probability of nonexceedence vs. repair cost for the three earthquake intensities. As expected the probability of nonexceedence of the original structure is significantly smaller than those of the retrofitted structures. It

Table 5
Replacement cost of the model structures (\$).

	Original structure	Increased section and SD	Increased section and HD	Structure with SD	Structure with HD
Total replacement cost (\$)	6,712,200	7,349,658	7,360,158	6,844,200	6,877,200
Core and shell replacement cost (\$)	2,684,880	2,939,863	2,944,063	2,737,680	2,750,880

Table 6
Mean repair costs required for the model structures (\$).

	Mean repair costs, (Mean Repair Cost/Total Replacement Cost (%))		
	Intensity1	Intensity2	Intensity3
Original structure	215,337(3.2%)	3,710,039(55.3%)	5,919,728(88.2%)
Structure with increased sections and SD	105,834(1.4%)	432,124(5.9%)	797,362(10.8%)
Structure with increased section and HD	103,586(1.4%)	305,946(4.1%)	734,664(9.9%)
Structure with SD	138,846(2.0%)	490,614(7.2%)	990,953(14.5%)
Structure with HD	144,904(2.1%)	388,595(5.7%)	924,093(13.4%)

Table 7
Mean repair time of each structure.

	Mean repair time in days (Mean repair/Total replacement Time)		
	Intensity1	Intensity2	Intensity3
Original structure	83(41.7%)	168(84.2%)	194(97.0%)
Structure with increased sections and SD	66(29.0%)	148(64.4%)	179(78.2%)
Structure with increased section and HD	58(25.7%)	138(60.1%)	170(74.3%)
Structure with SD	88(41.1%)	167(78.0%)	192(89.4%)
Structure with HD	72(33.9%)	146(68.2%)	182(85.0%)

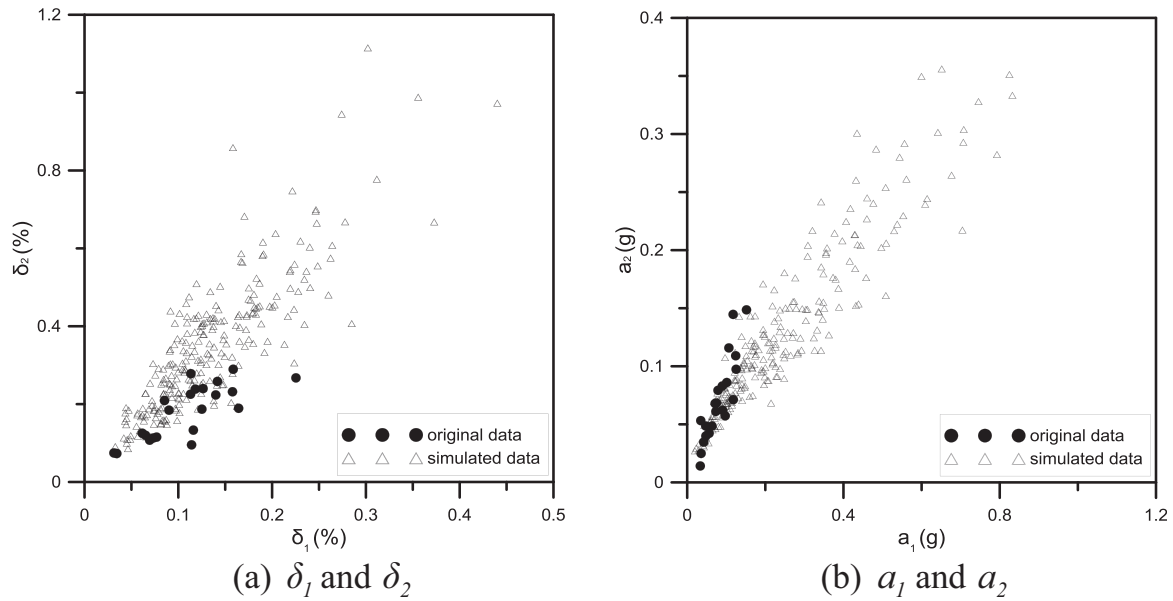


Fig. 17. Plots illustrating the correlation relationship between the maximum inter-story drifts of the first story (δ_1) and the second story (δ_2) and the acceleration of the first story (a_1) and the second story (a_2) at Intensity 1 earthquake.

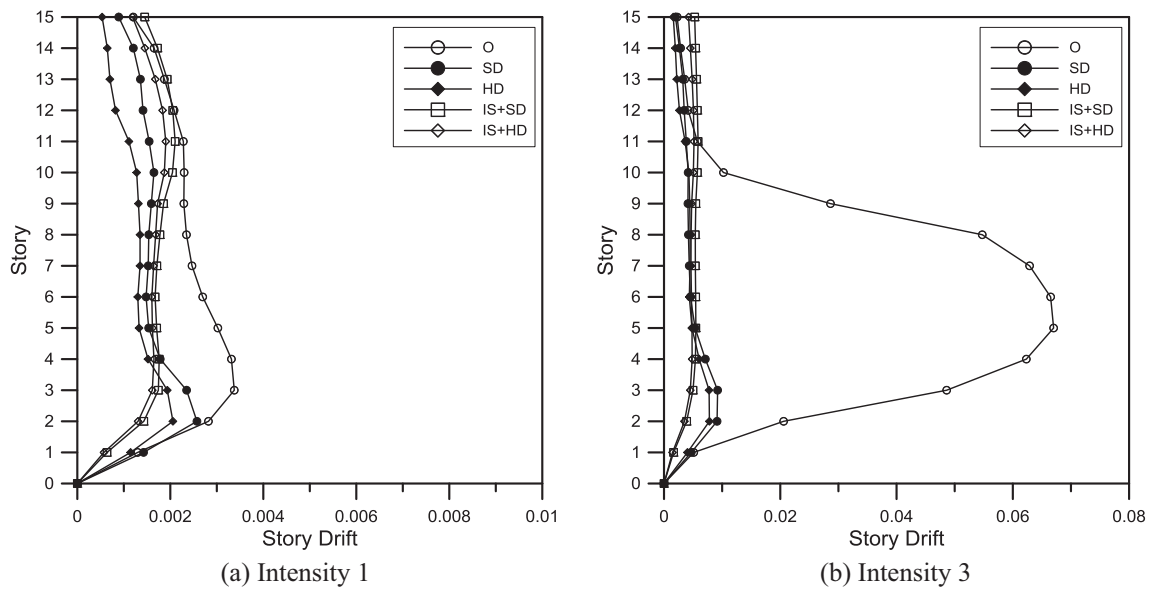


Fig. 18. Mean story drifts of the 500 simulated realizations.

can be observed that for a given repair cost the probability of nonexceedence is larger (i.e. the probability of exceedence is smaller) in the structure retrofitted with dampers after increasing column sizes (model IS + HD or IS + SD) than in the structure retrofitted only with dampers. As the earthquake intensity increases, the damage in the original structure increases rapidly and the probability of nonexceedence decreases significantly. It also can be noticed that the difference between the probabilities of nonexceedence of the original and the retrofitted structures also increases as the earthquake intensity increases.

The mean repair costs averaged over 500 realizations generated by the Monte Carlo simulation are presented in Table 6. The mean repair cost of the original structure for seismic event of Intensity 1

turns out to be 3.2% of the total replacement cost, whereas those of the structure retrofitted with slit or hybrid dampers after increase of column sections are smallest value of 1.4%. It is interesting to note that, even though the unit cost of hybrid damper is higher than that of the slit damper, the repair costs are identical at this seismic intensity. For Intensity 2 earthquakes the repair cost for the original structure increases to 55.3% of the total replacement cost, and the structure with increased section and HD results in the smallest value of 4.1%. Compared with the repair costs for earthquakes with lower intensity, the difference in the repair costs of the structure before and after the retrofit increases significantly for medium intensity earthquakes. For Intensity 3 earthquakes the repair cost for the original structure increases to 88.2% of the total

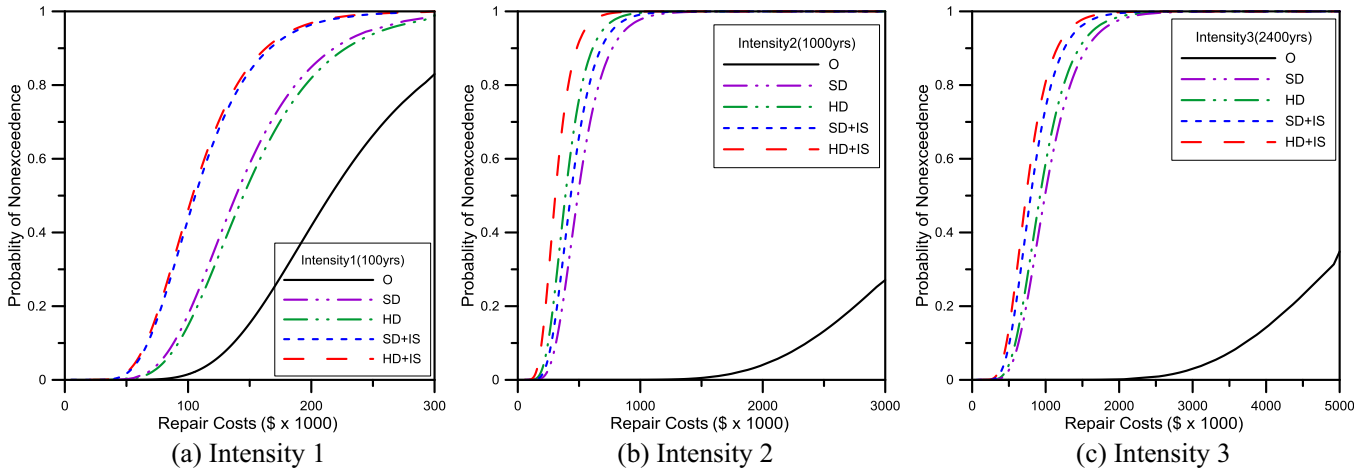


Fig. 19. Cumulative distribution of repair costs at various earthquake intensities.

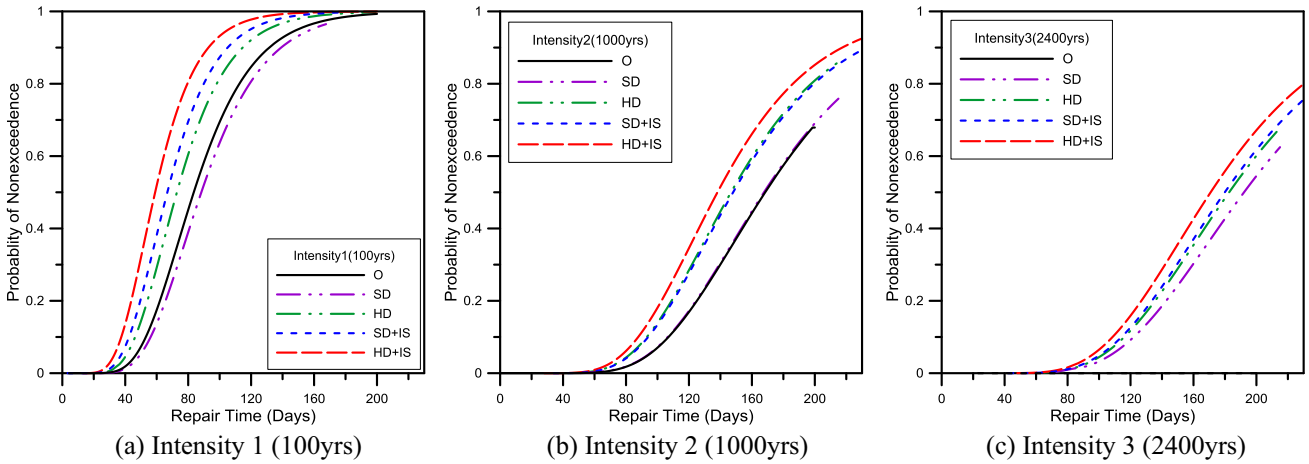


Fig. 20. Cumulative distribution of repair time at various earthquake intensities.

replacement cost while the retrofit with increased section and HD results in the minimum value is 9.9%. The retrofit with increased section and SD results in slightly higher repair cost. Therefore the retrofit scheme of increased column section with HD results in the lowest repair cost for earthquakes with all intensities.

Table 7 shows the mean repair time for the model structures when they are subjected to the earthquakes with three different intensities. It can be observed that, for Intensity 1 earthquakes, the repair time for the original structure is 88 days which is 41.7% of the total replacement time. The repair time for the structure with SD has similar repair time of 83 days. The structure retrofitted with increasing column size and HD (IS + HD) shows the shortest repair time of 58 days (25.7% of the replacement time). For Intensity 2 earthquakes, the repair time for the original and the retrofitted structure with IS + HD turns out to be the maximum of 168 days and the minimum of 138 days, respectively. The retrofitted structure with SD shows similar repair time to that of the original structure. For the earthquakes with Intensity 3, the repair time for the original structure is 194 days (97.0% of the replacement time) and the repair time for the model IS + HD is 170 days (74.3% of the replacement time). It is also observed that, for all earthquake intensities, the retrofit with increased section size with HD results in the shortest repair time, and that the repair time for the structure retrofitted only with HD is smaller than that for the structure retrofitted only with SD.

6. Conclusions

In this study a hybrid energy dissipation device was developed by attaching friction pads at both sides of a steel slit plate to be used for seismic retrofit of structures. Its seismic performance was validated by cyclic loading tests, and the effectiveness was investigated by comparing the life cycle cost and repair time of the structure before and after the retrofit using the FEMA P-58 methodology. This study also investigated the feasibility of simultaneous implementation of column jacketing and energy dissipation devices.

The fragility analysis shows that the probabilities of reaching limit states are minimized by the seismic retrofit with hybrid dampers and increasing column size at the same time. The mean repair cost of the original structure for seismic event of Intensity 1 turns out to be 3.2% of the total replacement cost, whereas those of the structure retrofitted with slit or hybrid dampers plus increase of column sections are smallest value of 1.4% of the total replacement cost. For Intensity 3 earthquakes the repair cost for the original structure increases to 88.2% of the total replacement cost while the retrofit with increased section and hybrid dampers results in the minimum value is 9.9%. It was also observed that, for Intensity 1 earthquakes, the repair time for the original structure is 41.7% of the total replacement time. The structure retrofitted with increasing column size and hybrid dampers showed the shortest repair

time of 25.7% of the replacement time. For the earthquakes with Intensity 3, the retrofit with increased section size with hybrid dampers resulted in the shortest repair time. Based on the fragility and life cycle cost analyses it could be concluded that the slit-friction hybrid damper shows superior performance to the slit damper with the same yield strength for seismic retrofit of structures.

Column jacketing mainly increases stiffness and strength of the structure, whereas dampers generally works to increase energy dissipation capacity. Even though the two methods are rarely implemented simultaneously in practice, there is no technical difficulty for doing that. This study showed that, if carefully planned, simultaneous application of jacketing (adding stiffness) and dampers (energy dissipation) may minimize both the seismic fragility and life cycle cost of the retrofitted buildings.

Acknowledgement

This research was supported by a grant (16AUDP-B066083-04) from Architecture & Urban Development Research Program funded by Ministry of Land, Infrastructure and Transport of Korean government.

References

- [1] Xia C, Hanson RD. Influence of ADAS element parameters on building seismic response. *J Struct Eng ASCE* 1992;118(7):1903–18.
- [2] Park J, Lee J, Kim J. Cyclic test of buckling restrained braces composed of square steel rods and steel tube. *Steel Compos Struct* 2012;13:423–36.
- [3] Chan RWK, Albermani F. Experimental study of slit damper for passive energy dissipation. *Eng Struct* 2008;30(4):1058–66.
- [4] Oh SH, Kim YJ, Ryu HS. Seismic performance of steel structures with slit dampers. *Eng Struct* 2009;31(9):1997–2008.
- [5] Saffaria H, Hedayatb AA, Poorsadeghi Nejad M. Post-Northridge connections with slit dampers to enhance strength and ductility dampers to enhance strength and ductility dampers to enhance strength and ductility. *J Constr Steel Res* 2013;80(1):138–52.
- [6] Seo J, Kim Y, Hu J. Pilot study for investigating the cyclic behavior of slit damper systems with recentering shape memory alloy (SMA) bending bars used for seismic restrainers. *Appl Sci* 2015;5:187–208.
- [7] Lee CH, Lho SH, Kim DH, Oh J, Ju YK. Hourglass-shaped strip damper subjected to monotonic and cyclic loadings. *Eng Struct* 2016;119(15):122–34.
- [8] Lee CH, Ju YK, Min JK, Lho SH, Kim SD. Non-uniform steel strip dampers subjected to cyclic loadings. *Eng Struct* 2015;99(15):192–204.
- [9] Pall A, Pall R. Performance based design using pall friction dampers – an economical design solution. In: Proceedings, thirteenth world conference on earthquake engineering. Vancouver; 2004.
- [10] Mualla IH, Belev B. Performance of steel frames with a new friction damper device under earthquake excitation. *Eng Struct* 2002;24(3):365–71. [http://dx.doi.org/10.1016/S0141-0296\(01\)00102-X](http://dx.doi.org/10.1016/S0141-0296(01)00102-X).
- [11] Lee CH, Ryu J, Oh J, Yoo CH, Ju YK. Friction between a new low-steel composite material and milled steel for SAFE Dampers. *Eng Struct* 2016;122:279–95.
- [12] Tsai CS, Chen K-C, Chen C-S. Seismic resistibility of high-rise buildings with combined velocity-dependent and velocity-independent devices. In: 1998 ASME pressure vessels and piping conference, vol. 366. San Diego, CA, ASME, Fairfield (NJ); 1998, p. 103–110.
- [13] Chen C-S, Chen K-C, Pong WS, Tsai CS. Parametric study for buildings with combined displacement-dependent and velocity-dependent energy dissipation devices. *Struct Eng Mech* 2002;14(1):85–98.
- [14] Uetani K, Tsuji M, Takewaki I. Application of optimum design method to practical building frames with viscous dampers and hysteretic dampers. *Eng Struct* 2003;25:579–92.
- [15] Marko J, Thambiratnam D, Perera N. Influence of damping systems on building structures subject to seismic effects. *Eng Struct* 2004;26(13):1939–56.
- [16] Marshall JD, Charney FA. Seismic response of steel frame structures with hybrid passive control systems. *Earthquake Eng Struct Dynam* 2012;41(4):715–33.
- [17] Murakami Y, Noshi K, Fujita K, Tsuji M, Takewaki I. Simultaneous optimal damper placement using oil, hysteretic and inertial mass dampers. *Earthquakes Struct* 2013;5(3):261–76.
- [18] Lee J, Kim J. Seismic performance evaluation of moment frames with slit-friction hybrid dampers. *Earthquakes Struct* 2015;9(6):1291–311.
- [19] Lee CH, Kim J, Kim DH, Ryu J, Ju YK. Numerical and experimental analysis of combined behavior of shear-type friction damper and non-uniform strip damper for multi-level seismic protection. *Eng Struct* 2016;114(1):75–92.
- [20] FEMA. Seismic performance assessment of buildings: FEMA P–58, prepared by the applied technology council for the federal emergency management agency. Washington (DC); 2012.
- [21] FEMA 461. Interim testing protocols for determining the seismic performance characteristics of structural and nonstructural components. Redwood City, California: Applied Technology Council; 2007.
- [22] Whittaker AS, Bertero VV, Thompson CL, Alonso LJ. Seismic testing of steel-plate energy dissipating devices. *Earthquake Spectra* 1991;7(4):563–604.
- [23] AISC 341-10. Seismic provisions for structural steel buildings. Chicago, Illinois: American Institute of Steel Construction; 2010.
- [24] ASCE/SEI 41-13. American society of civil engineers. Seismic evaluation and retrofit of existing buildings. Reston; 2013.
- [25] Perform 3D. Computer and Structures, Inc. PERFORM User Guide ver 4; 2006.
- [26] Kim J, Jeong J. Seismic retrofit of asymmetric structures using steel plate slit dampers. *J Constr Steel Res* 2016;120:232–44.
- [27] ATC-40. Seismic evaluation and retrofit of concrete buildings: volume 1, Applied Technology Council, Redwood City, California 94065.
- [28] ASCE/SEI 7-13. American Society of Civil Engineers. Minimum Design Loads for Buildings and Other Structures: Reston; 2013.
- [29] Cornell CA, Jalayer F, Hamburger RO, Foutch DA. The probabilistic basis for the 2000 SAC/FEMA steel moment frame guidelines. *ASCE J Struct Eng* 2002;128(4):526–33.
- [30] PEER. PEER NGA Database. University of California, Berkeley (USA): Pacific Earthquake Engineering Research Center; 2006 <<http://peer.berkeley.edu/nga>>.
- [31] HAZUS-MH 2.1. Technical Manual, Federal Emergency Management Agency, Washington (DC, USA); 2010.
- [32] International Construction Cost Survey 2010–2011. Turner & Townsend; 2010.
- [33] RSMMeans Building Construction Cost Data. Waier, Phillip R. (EDT)/Babbitt, Christopher (EDT)/Baker, Ted (EDT)/Balboni, Barbara (EDT)/Bast 10; 2011.